JACS
JOURNAL OF THE AMERICAN CHEMICAL SOCIETY
pubs.acs.org/JACS
Article

Coupled Compositional and Displacive Modulations in $KLaMnWO_6$ Revealed by Atomic Resolution Imaging

Susana Garcia-Martin,* Graham King, Esteban Urones-Garrote, and Patrick M. Woodward*

Cite This: J. Am. Chem. Soc. 2021, 143, 19121−19127
Read Online
ACCESS | Metrics & More | Article Recommendations | Supporting Information

ABSTRACT: Complex compositional and displacive modulations of the crystal structure of $KLaMnWO_6$ are imaged with atomic resolution by means of scanning transmission electron microscopy (STEM). This oxide is stabilized by cation vacancies leading to a $La_{1+x/3}K_{1-x}MnWO_6$ stoichiometry. Compositional modulation on both the K and La layers are revealed in the high-angle annular dark-field STEM (HAADF-STEM) images. The compositional modulation within the La layer is coupled with the modulation of the octahedral tilting, which is exposed by imaging of the anion sublattice in annular bright-field STEM (ABF-STEM) images. These complex modulations are accommodated in a $5\sqrt{2}a_p \times 5\sqrt{2}a_p \times 2a_p$ perovskite-type structure.

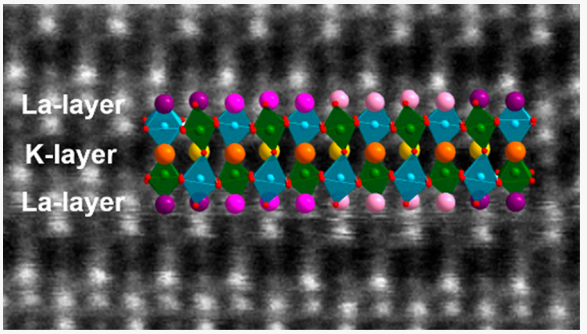

INTRODUCTION

The compositional diversity of substitutional derivatives of ABO_3 perovskites is a testament to the flexibility of the perovskite structure. Ordering at both A and B sites is a common mechanism to accommodate cations with different radii and/or oxidation states. In this context, simultaneous layered ordering of the A-site cations and rock-salt-type ordering with second-order Jahn−Teller distortions of the B-site cations stabilizes quintinary $AA'BB'O_6$ systems.[1,2] In addition to the coupled chemical ordering on the A and B sites, several compositions present an even more complex modulation of the crystal structure, including $NaLaMgWO_6$,[3] $KLaMnWO_6$,[4] $NaCe(Pr)MnWO_6$,[5] $NaLaCoWO_6$,[6] $K(Na)LaCaWO_6$,[7] and $NaNdMgWO_6$.[8] This modulation is also found in quaternary perovskites with layered ordering of the A sites such as $Nd_{2/3-x}Li_{3x}TiO_3$ and $La_{1/3-x}Li_{3x}NbO_3$,[9−11] suggesting a complicated interplay of structural aspects that is not fully understood. These modulations of the crystal structure, generally revealed by selected area electron diffraction (SAED) and high-resolution transmission electron microscopy (HRTEM), can be ascribed to compositional variations, modulated displacements of atoms, or a combination of the two.

In the case of the $Nd_{2/3-x}Li_{3x}TiO_3$, Guiton et al. concluded nanoscale compositional ordering arising from interparticle phase segregation into $Nd_{1/2}Li_{1/2}TiO_3$ and $Nd_{2/3}TiO_3$ coupled with periodic twinning of octahedral tilts to form domains in a chessboard like pattern.[11,12] Further investigations using a combination of techniques (mainly powder neutron diffraction and scanning transmission electron microscopy) opened an intense debate on the origin of the modulation of the crystal structure of these perovskites, supporting a displacive modulation of the octahedral tilting coupled to B-site cation displacements driven by second-order Jahn−Teller distortions.[13−20] However, the presence of a periodic modulation of the octahedral tilts does not preclude a compositional modulation. In fact, crystal chemistry considerations suggest that the two should be linked. We have demonstrated a compositional modulation of the La content in $NaLaMgWO_6$ and $KLaMnWO_6$ by means of electron energy loss spectroscopy (EELS). The nanostructured architectures consist of La-rich domains alternating with La-poor domains forming stripes in the case of $NaLaMgWO_6$ and a chessboard pattern in $KLaMnWO_6$. In addition, we suggested this compositional modulation to be coupled with a displacive modulation arising from periodic twinning of the tilts present in the network of corner-connected octahedra.[3,4] Despite the body of work performed to date, questions about the interplay between these various compositional and structural modulations remain unanswered.

Quaternary and quintenary perovskites with layered order are also of interest for their physical properties. In this context, high Li^+ conductivity has been reported in $Nd_{0.55}Li_{0.34}TiO_{3.00}$ and $La_{0.29}Li_{0.12}NbO_3$;[20,21] complex magnetic ordering has been found in $NaLnMnWO_6$ (Ln = lanthanide cations);[22,23] ferroelectricity and potential multiferroic behavior has been reported in $NaLaMnWO_6$;[24] and more recently, several

Received: August 19, 2021
Published: November 3, 2021

https://doi.org/10.1021/jacs.1c07426
J. Am. Chem. Soc. 2021, 143, 19121−19127

$AA'BB'O_6$ perovskites have been shown to be promising phosphor hosts when doped with appropriate lanthanoid ions.[25−30] Given that the crystal structure can have a significant impact on the physical properties of perovskite-type oxides, detailed knowledge of their structure is essential for understanding and predicting their physical behavior.

In this work, we revisit the origin of the modulation of the crystal structure of $KLaMnWO_6$. Using transmission electron microscopy with atomic resolution we have studied the periodic modulations of cation and anion occupancies and positions. The combination of Z-contrast imaging and EELS mapping reveals the locations of the cations in the crystal structure highlighting the compositional modulations, while mapping of the oxygen positions sheds new light on the periodic modulation of the octahedral tilting. The results presented here reveal the interplay between the compositional modulation and the modulation of the octahedral tilting.

EXPERIMENTAL SECTION

$KLaMnWO_6$ was prepared by the ceramic method using K_2CO_3 (Baker 99.9%), La_2O_3 (G. Frederick Smith 99.99%), and $MnWO_4$.[4] $MnWO_4$ was prepared from MnO (Cerac 99.9%) and WO_3 (Cerac 99.99%). A 5% excess of K_2CO_3 was used to account for the high-temperature volatility of this substance. Stoichiometric amounts of the reactants were ground together and heated at 1000 °C under a dynamic flow of forming gas (5% H_2, 95% N_2) for 8 h.

The average oxidation state of Mn and W atoms of the oxide was determined by EELS. In the case of manganese, the white-line ratio of the Mn-$L_{2,3}$ edge was evaluated,[31] whereas for tungsten, the W−$O_{2,3}$ edge position was studied.[32] In the latter case, the observed energy-loss values are around 37 and 39 eV, compatible with a 6+ oxidation state. The spectra were acquired in diffraction mode, with a dispersion of 0.1 eV per channel, a collection angle of $\beta \approx 5.3$ mrad, and an acquisition time of 2 s. The backgrounds of all the raw spectra were removed using a power-law model. When necessary, plural-scattering effects were removed by a Fourier-ratio deconvolution method.[33]

High-angle annular dark-field (HAADF) and annular bright-field (ABF) scanning transmission microscopy (STEM) work was performed on an ARM200cF microscope fitted with a condenser lens aberration corrector (point resolution in STEM mode of 0.08 nm). HAADF images were acquired with an inner acceptance angle of 90 mrad and ABF ones with a collection angle of 11 mrad. The same ARM200cF microscope was employed for EELS experiments, as it is fitted with a GIF Quantum-ER spectrometer. EELS mapping was performed with a collection semiangle $\beta \approx 30$ mrad, 0.5 eV per channel dispersion, and the collection time for each spectrum of 0.09 s. La-$M_{4,5}$, K-$L_{2,3}$, Mn-$L_{2,3}$, and W-$M_{4,5}$ edge signals were chosen for mapping.

RESULTS AND DISCUSSION

Our previous results by SAED and HRTEM on $KLaMnWO_6$[4] confirmed the layered-type ordering of the K and La and the rock-salt ordering between Mn and W. In addition, the SAED pattern along the $[001]_p$ zone axis (p refers to the cubic perovskite) revealed a complex modulation of the crystal structure also shown in the contrast differences of the corresponding HRTEM image (Figure S1). By construction of the reciprocal lattice, we proposed a $10a_p \times 10a_p \times 2a_p$ unit cell for the crystal structure (a_p is the lattice parameter of the simple cubic perovskite). EELS line-scans along both the $[100]_p$ and $[110]_p$ directions on crystals oriented along $[001]_p$ showed periodic variation of the La content, suggesting alternation of La-rich and La-poor nanodomains. Powder neutron diffraction experiments also indicated twinning of the octahedral tilting, where each twin boundary creates an in-phase tilt in what is otherwise an $a^-a^-c^0$ pattern of tilting. On the basis of those observations, we suggested a 2D model of La-rich domains ($La_{1+x/3}K_{1-x}MnWO_6$) of $5a_p \times 5a_p$ dimensions alternating with La-poor domains (probably $LaKMnWO_6$) of the same dimensions, forming a chessboard type architecture. This compositional modulation is coupled with twinning of the octahedral tilting system.[4]

Figure 1a shows a HAADF-STEM image (Z contrast image) of a crystal of $KLaMnWO_6$ along the $[001]_p$ zone axis. This orientation of the crystal does not allow distinguishing either the layered ordering of La and K or the rock-salt ordering of Mn and W. However, brighter squarelike domains alternate with darker domains to form a kind of chessboard pattern. The brighter domains indicate a higher content of the heavier atoms than the darker domains that surround them. This intensity variation is shown in the line intensity profile (Figure 1b). Figure 1b also shows the periodic variation in the intensity of the La-$M_{4,5}$ edge signal obtained from an EELS line-scan along the $[110]_p$ direction on the columns of atoms indicated by the yellow line in the image, which confirms the La-content modulation with a periodicity of ~28.3 Å = $5\sqrt{2}a_p$).

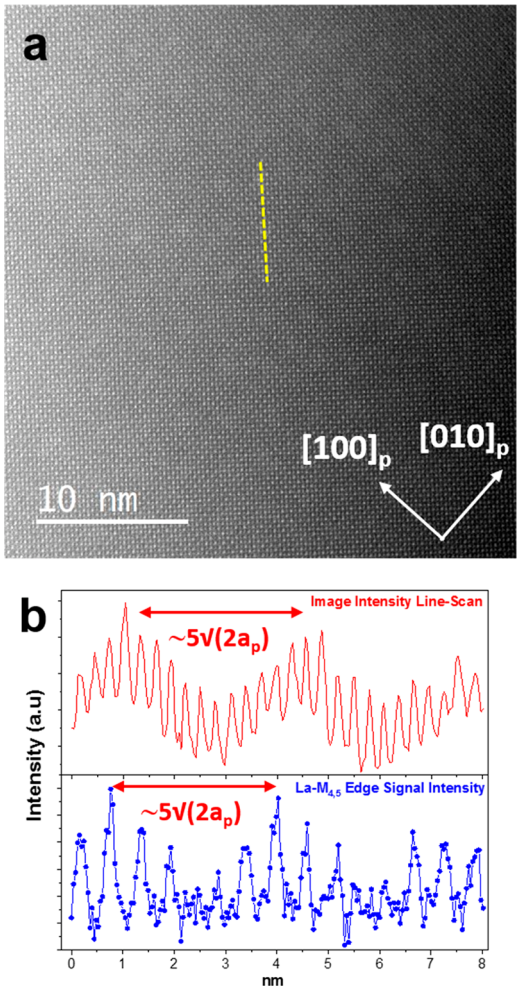

Figure 1. (a) HAADF-STEM image along the $[001]_p$ zone axis of a crystal of $KLaMnWO_6$. (b) Intensity variation profile and variation of the intensity of the La $M_{4,5}$ edge signal obtained from EELS line-scans along the yellow dotted line on the image.

The $[\bar{1}10]_p$ orientation of the crystal reveals information about the ordering of the atoms within the different layers

https://doi.org/10.1021/jacs.1c07426
J. Am. Chem. Soc. 2021, 143, 19121−19127

along the *c*-axis. Figure 2a depicts the HAADF-STEM image of a crystal of $KLaMnWO_6$ along the $[\bar{1}10]_p$ zone axis. The

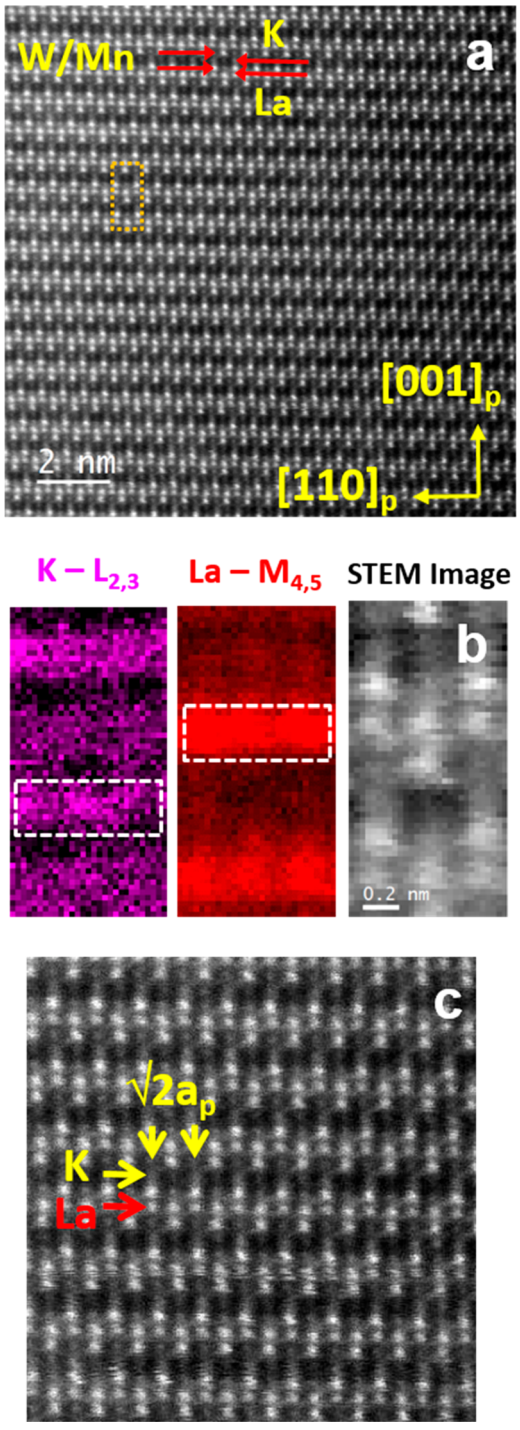

Figure 2. (a) HAADF-STEM image along the $[-110]_p$ zone axis of a crystal of $KLaMnWO_6$. (b) EELS maps of the orange marked area of the crystal in panel a. (c) Magnified area of the STEM image in panel a indicating the $\sqrt{2}a_p$ periodicity within the K layers.

contrast is characteristic of layered ordering of the A-site atoms and rock-salt ordering of the B-site atoms. EELS maps in Figure 2b confirm that layers of columns of La atoms alternate with layers of columns of K atoms along the $[001]_p$ direction, in agreement with the layered ordering of these atoms. EELS maps also confirm that columns of Mn atoms alternate with columns of W atoms along the $[110]_p$ and $[001]_p$ directions, in agreement with the rock-salt ordering of these atoms (Figure S2). However, the EELS maps in Figure 2b reveal that La and K are not completely distributed in separated layers but that the La layers contain a slight amount of K and the K layers also contain La. Furthermore, the K layers in Figure 2a, c show brighter and darker columns of atoms intercalated along the $[110]_p$ direction. This contrast variation leads to a $\sqrt{2}a_p$ periodicity, which coincides with the periodicity arising from the Mn and W ordering. The intensity profiles of the La-$M_{4,5}$ edge and K-$L_{2,3}$ edges of the EELS maps within the K layers along $[110]_p$ show intensity maxima coincident in the same positions (Figure S3), indicating that the $\sqrt{2}a_p$ periodicity is not associated with the K/La ordering within the K layer. This result is not surprising given the very small amount of La within the K layers. Therefore, the intensity variation of the K layer along the $[110]_p$ direction with a $\sqrt{2}a_p$ periodicity must be caused by ordering of cation vacancies, where the darker columns of atoms have a higher concentration of vacancies than do the lighter columns.

The compositional modulation at the K layers does not explain the superlattice reflections in the SAED patterns of this compound related to a modulation of the crystal structure with an $\sim 10a_p$ periodicity along both the $[100]_p$ and $[010]_p$ directions and $5\sqrt{2}a_p$ periodicity along the $[110]_p$ direction. On the contrary, the line intensity profiles and La-$M_{4,5}$ edge signal from EELS line scans that run along $[110]_p$ coincident with the La layers reveal that this modulation is associated with variation in the La content. Figure 3a shows another HAADF-STEM image of a crystal of $KLaMnWO_6$ along the $[\bar{1}10]_p$ zone axis and Figure 3b shows the corresponding image that has been processed to highlight the brightness variation as explained in Figure S4. The line intensity profile along $[110]_p$ within the La layer, indicated by the yellow dotted line, shows a periodic variation of ~28.3 Å $\approx 5\sqrt{2}a_p$, similar to the variation in the La content obtained from the La-$M_{4,5}$ edge signal from EELS line scans (Figure 1b). This $\sim 5\sqrt{2}a_p$ periodicity is in agreement with the modulation revealed from the satellite reflections around the main Bragg reflections in the SAED pattern of the $[001]_p$ zone axis (Figure S1). Associated with the modulation of the La content, there is a subtle modulation of the La−La distances (Figure S5).

Compositional modulation along $[110]_p$ has also been reported in the $La_{1/3-x}Li_{3x}NbO_3$ system.[34,35] Incommensurate modulations with periodicity $\sim 3.5\sqrt{2}a_p$ and $\sim 3.7\sqrt{2}a_p$ have been described in the cases of $x = 0$ and 0.04, respectively, associated with ordering of La, Li, and cation vacancies. In $KLaMnWO_6$, we find alternating $(001)_p$ La layers (that contain a small amount of K) and $(001)_p$ K/vacancy layers (that contain a small amount of La). On top of that, there are additional modulations within each layer, one along the $[110]_p$ direction in the K/vacancy layer with $\sqrt{2}a_p$ periodicity and another in the La layer with an $\sim 5\sqrt{2}a_p$ periodicity.

Figure 4 depicts schematic representations of the above-mentioned modulations in the $KLaMnWO_6$ with perovskite-related structure along different projections. The modulation in the La-rich layers can be described as an $\sim 10a_p$ periodicity along the $[100]_p$ and $[010]_p$ directions that leads to an $\sim 5\sqrt{2}a_p$ periodicity along the $[110]_p$ direction (Figure 4a, c). This modulation is in agreement with the contrast differences forming a chessboard pattern observed in both the HRTEM and HAADF-STEM images of the $[001]_p$ zone axis. The modulation in the K/vacancy layers has a shorter repeat

https://doi.org/10.1021/jacs.1c07426
J. Am. Chem. Soc. 2021, 143, 19121−19127

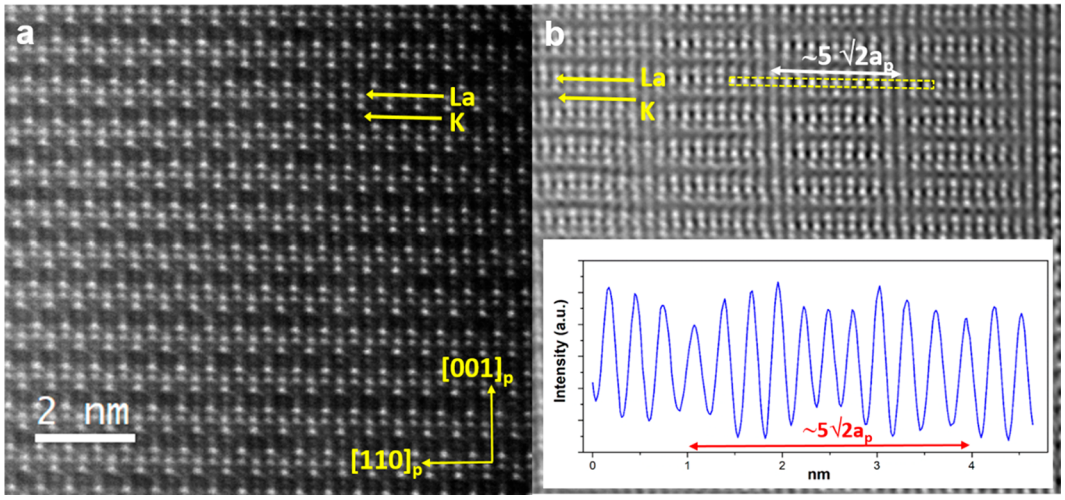

Figure 3. (a) HAADF-STEM image along the $[-110]_p$ zone axis of a crystal of $KLaMnWO_6$. (b) Image a after processing: the contrast of the $\sim 5\sqrt{2}a_p$ modulation is enhanced (see Figure S4 for details). The inset shows the intensity profile of the scan along the La layer, indicated by the yellow dotted line in the image.

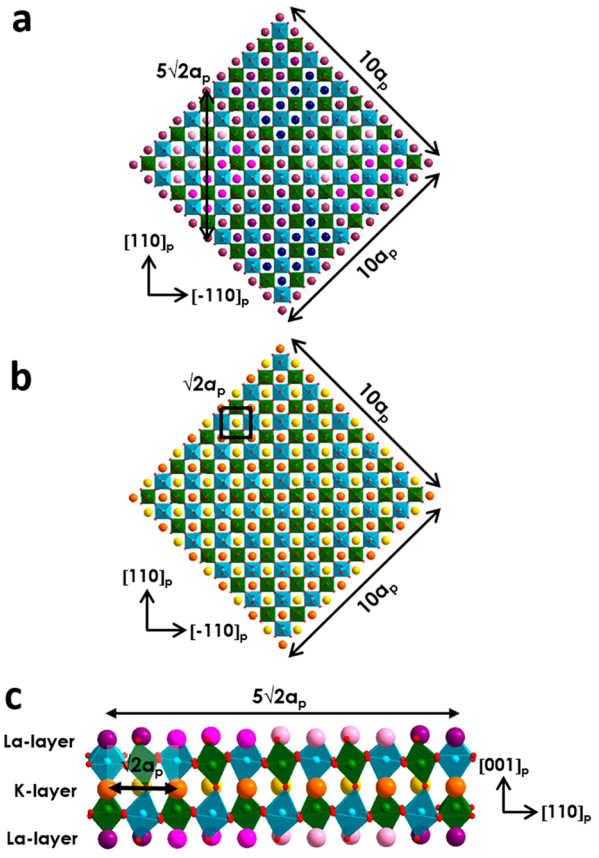

Figure 4. Schematic representation of the crystal structure along the $[001]_p$ projection: (a) one La layer; (b) one K layer. The different colors of the A positions represent different La content within the La layer. Colors going from dark blue to light pink represent the highest to the lowest occupation of La sites. The orange spheres represent K(La) sites and the yellow spheres represent K(La)/vacancies sites. (c) Schematic representation of the crystal structure along the $[\bar{1}10]_p$ projection.

distance of $\sim 2a_p$ along both the $[100]_p$ and $[010]_p$ directions, which leads to an $\sim\sqrt{2}a_p$ periodicity along $[110]_p$. Interestingly, this modulation is coincident with the rock-salt-type ordering of the Mn and W atoms (Figure 4b).The BF-STEM images provide information about the anion sublattice. Figure 5 shows ABF-STEM images of a crystal along the $[001]_p$ zone axis. Optimization of the image intensity after processing (Figure S6) highlights the intensity of the columns of oxygen atoms. There are domains showing wavy O−(Mn/W)−O columns of atoms in agreement with oxygen-octahedra tilting and domains in which the columns of oxygen atoms seem to form a regular nontilted octahedra around the Mn/W atoms. Moreover, the areas showing strong octahedra tilting are those brighter squarelike domains that indicate higher content of the heaviest atoms (the La-rich domains). A similar anion sublattice pattern was found in $Li_{3x}Nd_{2/3-x}TiO_3$.[14]

In this system, Abakumov et al. suggested areas with out-of-phase a^-b^- tilting with a pronounced c-tilt component ($a^-b^-c^+$) that interleave with areas where the c-tilt is suppressed. A modulation of the tilting of the oxygen octahedral network from the $a^-b^-c^0$ system to the $a^0b^0c^+$ system near twin boundaries was further proposed for $Li_{0.38}Nd_{0.54}TiO_3$.[15] In our previous work,[4] we also proposed a twinned $a^-a^-c^0$ tilting system for the average structure. The present study is consistent with a picture where $a^-b^-c^+$ tilting is present, but there is a modulation of the c^+ tilting that produces regions where the c^+ tilt is significant (regions with the highest La content) and regions where the c^+ tilting is suppressed (regions with the lowest La content). Out-of-phase a^-b^- tilting is present throughout the crystal, although the magnitude of the out of phase tilts are probably different in those regions where the c^+ tilting is suppressed than they are where the c^+ tilting is prominent.

Taking into account these results, we have to consider that $KLaMnWO_6$ is not the correct formula of our compound but $La_{1+x/3}K_{1-x}MnWO_6$. The oxidation states of Mn^{2+} and W^{6+} determined by EELS experiments (see Experimental Section) support the formation of A-site vacancies and hence the $La_{1+x/3}K_{1-x}MnWO_6$ stoichiometry. This oxide presents A-site vacancies mainly located within the K layers in such a way that K, La, and vacancies are ordered, resulting in a $\sqrt{2}a_p$ periodicity. The compositional modulation with a $5\sqrt{2}a_p$ periodicity along the $[110]_p$ direction is associated with

https://doi.org/10.1021/jacs.1c07426
J. Am. Chem. Soc. 2021, 143, 19121−19127

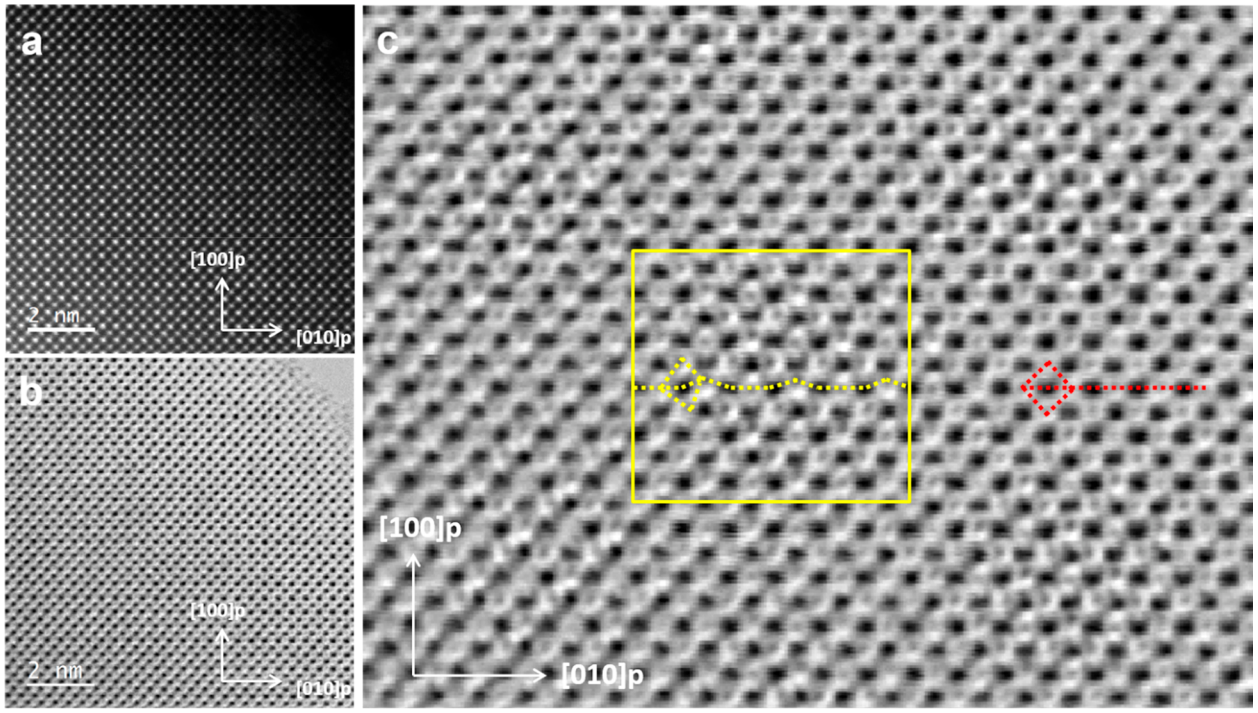

Figure 5. (a) HAADF-STEM image and (b) ABF-STEM image along the $[001]_p$ zone axis of a crystal of $KLaMnWO_6$. (c) ABF-STEM image b after processing: the contrast of the columns of oxygen atoms is enhanced (see Figure S6 for details). The yellow lines represent the wavy O−(Mn/W)−O columns of atoms due to oxygen-octahedra tilting and the red lines represent the regular nontilted octahedra around the Mn/W atoms.

periodic variations in the La content in the La-rich layers, which is accommodated with the incorporation of some K. These compositional modulations are coupled with a periodic twinned modulation of the octahedra tilts as shown in Figure 6

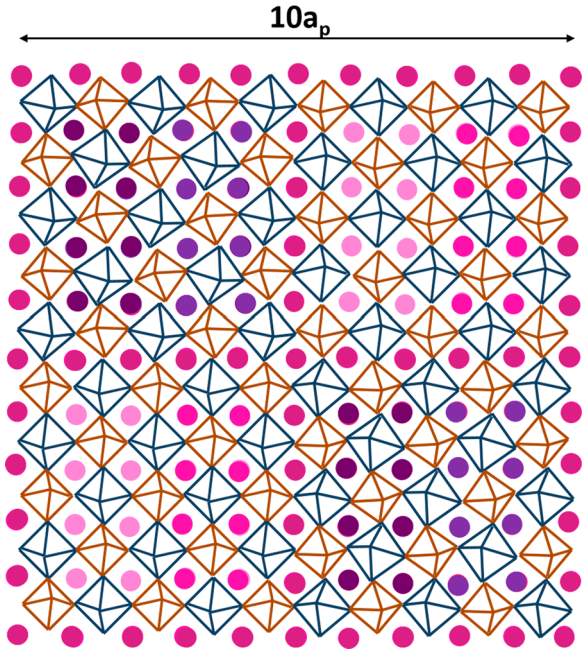

Figure 6. Schematic representation of the composition within the La-layer modulation coupled with a periodic twinned modulation of the octahedra tilts along the $[001]_p$ projection. The different colors of the A positions represents different La content within the La layer. Colors going from dark blue to light pink represent the highest to the lowest occupation of La sites.

and Figure S7. The variation in A-site volume created by the tilting modulation is intimately linked to the compositional modulation, as ultimately the size of the A-site cation drives the octahedral tilting distortion. Figure 6 and Figure S7 reflect the chessboard type pattern of the modulated structure.

CONCLUSIONS

Stabilization of $KLaMnWO_6$ with a perovskite-related structure involves formation of A-site vacancies, consistent with the general formula $La_{1+x/3}K_{1-x}MnWO_6$, and a complex compositional and displacive modulation of the crystal structure. The perovskite superstructure that results from simultaneous layered-type ordering of the La and K atoms and rock-salt-type ordering of the Mn and W atoms accommodates additional ordering within both the A-site layers in a $5\sqrt{2}a_p \times 5\sqrt{2}a_p \times 2a_p$ unit cell. The cation vacancies are mainly incorporated within the K layers causing a $\sqrt{2}a_p$ periodic ordering along $[110]_p$, which coincides with the periodic rock-salt ordering. The long modulation of the crystal structure with $5\sqrt{2}a_p$ periodicity also along $[110]_p$, is ascribed to a compositional modulation within the La layer. The $a^-b^-c^+$ tilting of the corner-connected octahedral network undergoes a modulation of the c^+ tilting that is coupled to the compositional modulation in the La layers. This coupling of the modulations is related to local crystal chemistry considerations, as tilting is driven by the fit of the A-site cations within the perovskite structure.

ASSOCIATED CONTENT

Supporting Information

The Supporting Information is available free of charge at https://pubs.acs.org/doi/10.1021/jacs.1c07426.

(Figure S1) SAED pattern and HRTEM image along the $[010]_p$ zone axis of a crystal of $KLaMnWO_6$; (Figure S2)

https://doi.org/10.1021/jacs.1c07426
J. Am. Chem. Soc. 2021, 143, 19121−19127

HAADF-STEM image along the $[-110]_p$ zone axis and EELS maps of a crystal of $KLaMnWO_6$; (Figure S3) HAADF-STEM image along the $[\bar{1}10]_p$ zone axis of a crystal of $KLaMnWO_6$; (Figure S4) process steps of a HAADF-STEM image of a crystal of $KLaMnWO_6$ along the $[\bar{1}10]_p$ zone axis; (Figure S5) processed HAADF-STEM image of a crystal of $KLaMnWO_6$ along the $[\bar{1}10]_p$ zone axis; (Figure S6) process steps of a ABF-STEM image along the $[001]_p$ zone axis of a crystal of $KLaMnWO_6$; (Figure S7) schematic representation of the compositional modulation within the La layer coupled with a periodic twinned modulation of the octahedra tilts along the $[001]_p$ projection (PDF)

AUTHOR INFORMATION

Corresponding Authors

Susana Garcia-Martin − *Departamento de Química Inorgánica. Facultad de Ciencias Químicas, Universidad Complutense, Madrid 28040, Spain;* orcid.org/0000-0003-0729-4892; Email: sgmartin@ucm.es

Patrick M. Woodward − *Department of Chemistry and Biochemistry, Ohio State University, Columbus, Ohio 43210, United States;* orcid.org/0000-0002-3441-2148; Email: woodward@chemistry.ohio-state.edu

Authors

Graham King − *Canadian Light Source, Saskatoon, Saskatchewan S7N 2V3, Canada;* orcid.org/0000-0003-1886-7254

Esteban Urones-Garrote − *Departamento de Química Inorgánica. Facultad de Ciencias Químicas, Universidad Complutense, Madrid 28040, Spain*

Complete contact information is available at: https://pubs.acs.org/10.1021/jacs.1c07426

Author Contributions

The manuscript was written through contributions of all authors. All authors have given approval to the final version of the manuscript.

Notes

The authors declare no competing financial interest.

ACKNOWLEDGMENTS

This work has been supported by the Spanish MICINN. We thank the Agencia Estatal de Investigación (AEI)/Fondo Europeo de Desarrollo Regional (FEDER/UE) for funding the Project PID2019-106662RB-C44. We acknowledge the Microscopy Centre of the UCM for providing facilities. P.M.W. acknowledges support from the Center for Emergent Materials: an NSF MRSEC under award DMR-2011876.

REFERENCES

(1) King, G.; Thimmaiah, S.; Dwivedi, A.; Woodward, P. M. Synthesis and Characterization of New $AA'BWO_6$ Perovskites Exhibiting Simultaneous Ordering of *A*-Site and *B*-Site Cations. *Chem. Mater.* **2007**, *19*, 6451.

(2) King, G.; Garcia-Martin, S. Expanding the Doubly Cation Ordered $AA'BB'O_6$ Perovskite Family: Structural Complexity in $NaLaInNbO_6$ and $NaLaInTaO_6$. *Inorg. Chem.* **2019**, *58*, 14058−14067.

(3) Garcia-Martin, S.; Urones-Garrote, E.; Knapp, M. C.; King, G.; Woodward, P. M. Transmission Electron Microscopy Studies of $NaLaMgWO_6$: Spontaneous Formation of Compositionally Modulated Stripes. *J. Am. Chem. Soc.* **2008**, *130*, 15028−15037.

(4) Garcia-Martin, S.; King, G.; Urones-Garrote, E.; Nenert, G.; Woodward, P. M. Spontaneous Superlattice Formation in the Doubly Ordered Perovskite $KLaMnWO_6$. *Chem. Mater.* **2011**, *23*, 163−170.

(5) Garcia-Martin, S.; King, G.; Nenert, G.; Ritter, C.; Woodward, P. M. The Incommensurately Modulated Structures of the Perovskites $NaCeMnWO_6$ and $NaPrMnWO_6$. *Inorg. Chem.* **2012**, *51*, 4007−4014.

(6) Zuo, P.; Darie, C.; Colin, C. V.; Klein, H. Investigation of the Structure of the Modulated Doubly Ordered Perovskite NaLaCoWO6 and Its Reversible Phase Transition with a Colossal Temperature Hysteresis. *Inorg. Chem.* **2019**, *58* (1), 81−92.

(7) Licurse, M. W.; Borisevich, A. Y.; Davies, P. K. Nanoscale modulations in $(KLa)(CaW)O_6$ and $(NaLa)(CaW)O_6$. *J. Solid State Chem.* **2012**, *191*, 220−224.

(8) Licurse, M. W.; Davies, P. K. Nanocheckerboard modulations in $(NaNd)(MgW)O_6$. *Appl. Phys. Lett.* **2010**, *97*, 123101.

(9) Garcıa-Martin, S.; Garcıa-Alvarado, F.; Robertson, A.D.; West, A.R.; Alario-Franco, M.A. Microstructural Study of the Li^+ Ion Substituted Perovskites $Li_{0.5-3x}Nd_{0.5+x}TiO_3$. *J. Solid State Chem.* **1997**, *128*, 97−101.

(10) Guiton, B. S.; Davies, P. K. Spontaneous Compositional Nanopatterning in Li-Containing Perovskite Oxides. *J. Am. Chem. Soc.* **2008**, *130*, 17168−17173.

(11) Garcia-Martin, S.; Alario-Franco, M.A. Modulated Structure of $La_{1/3-x}Li_{3x}NbO_3$ $0 \le x \le 0.06$ Perovskite-Related Materials. *J. Solid State Chem.* **1999**, *148*, 93−99.

(12) Guiton, B. S.; Wu, H.; Davies, P. K. Neutron Powder Diffraction of $(Nd_{7/12}Li_{1/4})TiO_3$ Nano-Checkerboard Superlattices. *Chem. Mater.* **2008**, *20*, 2860−2862.

(13) Withers, R. L.; Bourgeois, L.; Snashall, A.; Liu, Y.; Noren, L.; Dwyer, C.; Etheridge, J. Chessboard/Diamond Nanostructures and the A-site Deficient, $Li_{1/2-3x}Nd_{1/2+x}TiO_3$, Defect Perovskite Solid Solution. *Chem. Mater.* **2013**, *25*, 190−201.

(14) Abakumov, A. M.; Erni, R.; Tsirlin, A. A.; Rossell, M. D.; Batuk, D.; Nenert, G.; Tendeloo, G. V. Frustrated Octahedral Tilting Distortion in the Incommensurately Modulated $Li_{3x}Nd_{2/3-x}TiO_3$ Perovskites. *Chem. Mater.* **2013**, *25*, 2670−2683.

(15) Zhu, Y.; Withers, R. L.; Bourgeois, L.; Dwyer, C.; Etheridge, J. Direct mapping of Li-enabled octahedral tilt ordering and associated strain in nanostructured perovskites. *Nat. Mater.* **2015**, *14*, 1142−1149.

(16) Garcia-Martin, S.; Urones-Garrote, E.; King, G.; Woodward, P. Comment on Frustrated Octahedral Tilting Distortion in the Incommensurately Modulated $Li_{3x}Nd_{2/3-x}TiO_3$ Perovskites. *Chem. Mater.* **2014**, *26*, 1286−1287.

(17) Abakumov, A. M.; Erni, R.; Tsirlin, A. A. Reply to Comment on Frustrated Octahedral Tilting Distortion in the Incommensurately Modulated $Li_{3x}Nd_{2/3-x}TiO_3$ Perovskites. *Chem. Mater.* **2014**, *26*, 1288.

(18) Erni, R.; Abakumov, A. M.; Rossell, M. D.; Batuk, D.; Tsirlin, A. A.; Nenert, G.; Van Tendeloo, G. Nanoscale phase separation in perovskites revisited. *Nat. Mater.* **2014**, *13*, 216−217.

(19) Davies, P. K.; Guiton, B. S. Reply to 'Nanoscale phase separation in perovskites revisited. *Nat. Mater.* **2014**, *13*, 217−218.

(20) Itoh, M.; Inaguma, Y.; Jung, W. H.; Chen, L.; Nakamura, T. High lithium ion conductivity in the perovskite-type compounds $Ln_{1/2}Li_{1/2}TiO_3$ (Ln = La,Pr,Nd,Sm). *Solid State Ionics* **1994**, *70-71*, 203−207.

(21) García-Martín, S.; Rojo, J. M.; Tsukamoto, H.; Morán, E.; Alario-Franco, M. A. Lithium-ion conductivity in the novel $La_{1/3-x}Li_{3x}NbO_3$ solid solution with perovskite-related structure. *Solid State Ionics* **1999**, *116*, 11−18.

(22) King, G.; Wayman, L. M.; Woodward, P. M. Magnetic and structural properties of $NaLnMnWO_6$ and $NaLnMgWO_6$ perovskites. *J. Solid State Chem.* **2009**, *182*, 1319−1325.

(23) King, G.; Wills, A. S.; Woodward, P. M. Magnetic structures of $NaLMnWO_6$ perovskites (*L*=La,Nd,Tb). *Phys. Rev. B: Condens. Matter Mater. Phys.* **2009**, *79*, 224428.

(24) Fukushima, T.; Stroppa, A.; Picozzi, S.; Perez-Mato, J. M. Large ferroelectric polarization in the new double perovskite $NaLaMnWO_6$ induced by non-polar instabilities. *Phys. Chem. Chem. Phys.* **2011**, *13*, 12186−12190.
(25) Sharits, A. R.; Khoury, J. F.; Woodward, P. M. Evaluating $NaREMgWO_6$ (RE = La, Gd, Y) Doubly Ordered Double Perovskites as Eu^{3+} Phosphor Hosts. *Inorg. Chem.* **2016**, *55*, 12383−12390.
(26) Ran, W.; Noh, H. M.; Moon, B. K.; Park, S. H.; Jeong, J. H.; Kim, J. H.; Liu, G.; Shi, J. Shi, Crystal structure, electronic structure and photoluminescence properties of $KLaMgWO_6$:Eu^{3+} phosphors. *J. Lumin.* **2018**, *197*, 270−276.
(27) Yang, Q.; Li, G.; Wei, Y.; Chai, H. Synthesis and photoluminescence properties of red-emitting $NaLaMgWO_6$:Sm^{3+},Eu^{3+} phosphors for white LED applications. *J. Lumin.* **2018**, *199*, 323−330.
(28) Ran, W.; Noh, H. M.; Park, S. H.; Lee, B. R.; Kim, J. H.; Jeong, J. H.; Shi, J. Er^{3+}-Activated $NaLaMgWO_6$ double perovskite phosphors and their bifunctional application in solid-state lighting and non-contact optical thermometry. *Dalton Trans.* **2019**, *48*, 4405.
(29) Kumar, K. N.; Vijayalakshmi, L.; Choi, J. Investigation of Upconversion Photoluminescence of Yb^{3+}/Er^{3+}:$NaLaMgWO_6$ Non-cytotoxic Double-Perovskite Nanophosphors. *Inorg. Chem.* **2019**, *58*, 2001−2011.
(30) Long, Z.; Xiao, S.; Yang, X. Mn^{4+}, Eu^{3+} Co-doped $K_{0.3}La_{1.233}MgWO_6$: A Potentially Multifunctional Luminescent Material. *ACS Appl. Electron. Mater.* **2020**, *2*, 3889−3897.
(31) Schmid, H. K.; Mader, W. Oxidation states of Mn and Fe in various compound oxide systems. *Micron* **2006**, *37* (5), 426−432.
(32) Bangert, U.; Zhou, X.; Iglesias-Rubianes, L.; Skeldon, P.; Thompson, G. E. EELS study of oxidation state of tungsten in anodic alumina film formed on Al−6·5 at.-%W alloy. *Trans. Inst. Met. Finish.* **2007**, *85*, 306−309.
(33) Egerton, R. F. *Electron Energy-Loss Spectroscopy in the Electron Microscope*, 3rd ed.; Springer International Publishing: 2011.
(34) Gao, X.; Fisher, C. A. J.; Ikuhara, Y. H.; Fujiwara, Y.; Kobayashi, S.; Moriwake, H.; Kuwabara, A.; Hoshikawa, K.; Kohama, K.; Iba, H.; Ikuhara, Y. Cation ordering in A-site-deficient Li-ion conducting perovskites $La_{(1-x)/3}Li_xNbO_3$. *J. Mater. Chem. A* **2015**, *3*, 3351−3359.
(35) Hu, X.; Kobayashi, S.; Ikuhara, Y. H.; Fisher, C. A.J.; Fujiwara, Y.; Hoshikawa, K.; Moriwake, H.; Kohama, K.; Iba, H.; Ikuhara, Y. Atomic scale imaging of structural variations in $La_{(1-x)/3}Li_xNbO_3$ ($0 \leq x \leq 0.13$) solid electrolytes. *Acta Mater.* **2017**, *123*, 167−176.

https://doi.org/10.1021/jacs.1c07426
J. Am. Chem. Soc. 2021, 143, 19121−19127